Characteristics of Rotationally Stabilized Long Plasma Arcs in a Chamber

HSU-CHIEH YEH AND WEN-JEI YANG
Department of Mechanical Engineering, The University of Michigan, Ann Arbor, Michigan 48104
(Received 4 November 1968; in final form 27 January 1969)

An analytical method is developed to determine the gas temperature distribution and the electric field strength-arc length characteristics of a rotationally stabilized long plasma arc in a cylindrical chamber. The application of the method was demonstrated by numerical computations which were carried out for a monatomic hydrogen arc stabilized in a very large chamber. The relationships among the electric field strength, current, arc length, and arc-axis temperature are disclosed.

INTRODUCTION

The problems of arc plasma heat transfer are in general complicated due to the temperature dependency of physical properties, which introduces nonlinearity into the governing differential equations. As a result, most of the theoretical works now available deal with simplified cases such as the wall stabilized long arcs with negligible convective effects in which temperature distribution may be considered to be dependent only on radial distance. For these simplified cases the principle of energy conservation may be expressed by the so called Elenbass–Heller equation

$$(1/r)(d/dr)[\lambda r(dT/dr)]+\sigma E^2=Q_r(T), \qquad (1)$$

where σ is the electric conductivity, E the strength of electric field, T the gas temperature, λ the thermal conductivity, and Q_r the radiation losses per unit volume. In case of monatomic gases, one may assume that Q_r is proportional to $(1/T)\exp(-eV_i/kT)$ and $\lambda=\lambda_0 T^\alpha$, where k is the Boltzmann constant, V_i the effective energy level of the atom, e the electron charge, λ_0 a reference value of λ, and α a constant. With the simplifying assumptions, the temperature distribution of the gas was obtained by the numerical integration of Eq. (1).[1–6] However, for the case of molecular gases, the dependency of λ, Q_r, and σ on the gas temperature is generally more complicated than that for the monatomic gas case. Nevertheless, Eq. (1) was numerically integrated for many instances in which the radiation losses were considered negligible and the λ–T relationship was known.[7–9] Analytical solution of Eq. (1) was first obtained by Maecker[10] through the use of the thermal-conduction potential defined as $S=\int\lambda dT$ and the linearization of the function $\sigma(S)$. His results agreed well with the experiments by Belousova and Gurevik[11] for a mercury arc. The similarity solution of the energy equation for a two-dimensional arc was obtained by Anderson and Eckert[12] under the assumption that the axial velocity component of the gas for a fully developed flow is a linear function of the axial distance.

Generally speaking, one can create a long arc in a small tube by virtue of the stabilizing effect of the tube wall. When a large-diameter tube is used, a long arc may be stabilized by the vortex flow around the arc.[13,14] This vortex flow may be induced by rotating a system of screens inside the arc chamber,[15] by a rotor with an impeller mounted on the shaft,[16] or by a continuous stream of the gas tangentially blown into the discharge chamber.[17] An arc as long as 25 cm was reported to have been produced with the use of needle electrodes. It is the purpose of this paper to study analytically the gas temperature distribution and the arc length–electric field strength characteristics of the rotationally stabilized long arc produced between two needle electrodes in a cylindrical chamber.

ANALYSIS

The physical system to be investigated is shown in Fig. 1. It consists of an arc (not shown) with length L between two needle electrodes confined in a cylindrical chamber in which a gas rotates around the arc. The chamber has a radius R and its wall temperature is maintained constant at T_2. The arc is comparatively long and is stabilized by the rapid rotation of the gas. Both the upper and lower electrodes are water cooled. A cylindrical coordinate system (r, z) is fixed at the center of the arc between the electrodes. The coordinate r measures the radial distance from the arc axis,

[1] W. Elenbass, Physics **1**, 673 (1934).
[2] G. Heller, Physics **6**, 389 (1935).
[3] G. Schmitz, Z. Physik **44**, 129 (1943).
[4] V. J. Francis, Phil. Mag. **37**, 433 (1946).
[5] G. Schmitz and W. Hocker, Z. Physik **129**, 104 (1951).
[6] O. Koch and H. Dunstader, Z. Physik **129**, 140 (1951).
[7] R. Mannkopff, Z. Physik **120**, 228 (1943).
[8] H. Maecker, Z. Physik **128**, 289 (1950).
[9] L. A. King, *Colloquium Spectroscopium Internationale, Amsterdam*, 1956 (Pergamon Press, Inc., London), p. 152.
[10] H. Maecker, Z. Physik **157**, 1 (1959).
[11] M. Belousova and D. B. Gurevik, Sov. Phys.—Tech. Phys. **6**, 974 (1962).
[12] J. E. Anderson and E. R. G. Eckert, AIAA J. **5**, 699 (1967).
[13] H. Maecker, Z. Physik **129**, 108 (1951).
[14] F. Burhorn, H. Maecker, and T. Peters, Z. Physik **131**, 28 (1951).
[15] E. S. Borovik, R. V. Mitin, and Yu. R. Knyazev, Sov. Phys.—Tech. Phys. **6**, 968 (1962).
[16] R. V. Mitin, Yu. R. Knyazev, and V. L. Petrenko, Sov. Phys.—Tech. Phys. **9**, 267 (1964).
[17] Yu. R. Knyazev, R. V. Mitin, V. I. Petrenko, and E. S. Borovik, Sov. Phys.—Tech. Phys. **9**, 948 (1965).

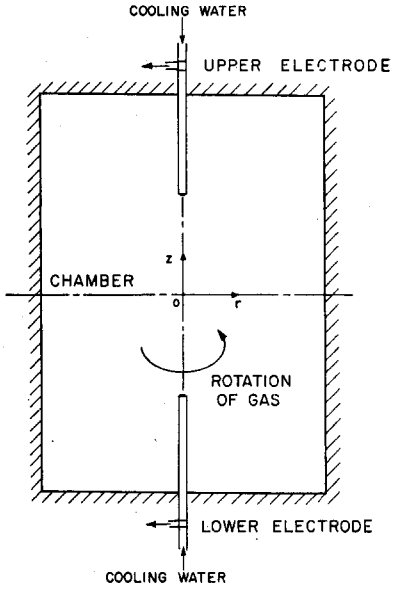

FIG. 1. Physical and coordinate systems.

while z measures the axial distance along the arc. Because of the rapid rotation of the gas, free convection induced by gravitation can be neglected. As a result, the gas temperature in the chamber is distributed symmetrically with respect to a plane through the origin and perpendicular to the arc axis. Since the flow of the gas is tangential, the convective heat transfer in the radial direction is negligible. Furthermore, since the temperature distribution is axisymmetric, the convective heat transfer in the azimuthal direction is also negligible. In other words, heat transfer performance is independent of the velocity of the gas rotation. This is evidenced by experiments[18] which revealed that the arc characteristics becomes independent of the gas rotation when the latter exceeds 2500 rpm. As far as radiation is concerned its effect is important only when both the gas pressure and power input are high. For the present analysis, which is concerned with low to moderate pressure ranges, the radiation effect will be ignored.

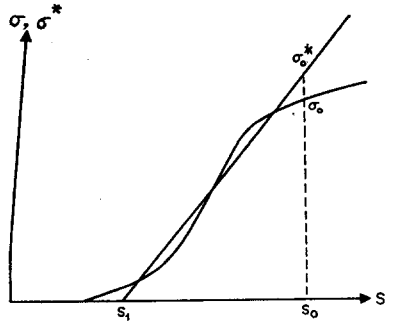

FIG. 2. Linearization of the σ–S relationship.

[18] C. G. Suits and H. Poritsky, Phys. Rev. 55, 1184 (1939).

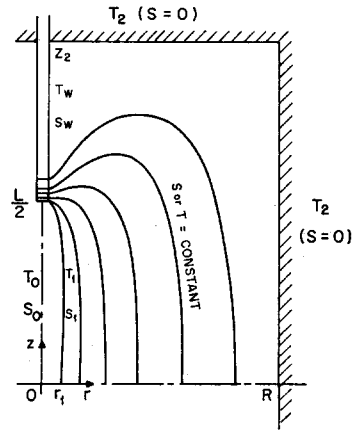

FIG. 3. Model for actual gas temperature distribution in an arc chamber.

Now, energy balance on the gas yields

$$\frac{1}{r}\frac{\partial r}{\partial r}\left(\lambda r\frac{\partial T}{\partial r}\right)+\frac{\partial}{\partial Z}\left(\lambda\frac{\partial T}{\partial z}\right)+\sigma E^2=0, \qquad (2)$$

where the first two terms represent the radial and axial components of thermal conduction, respectively, and the last term indicates the Joule heating. Before an attempt is made to solve the energy equation, the characteristic of E and σ will be examined

In general, both E and σ are functions of r as well as z. For a long arc, it is reasonable to assume that the constant current-density lines in the arc column are parallel to the axis except in the end regions near the electrodes. From Ohm's law $\mathbf{j}=\sigma\mathbf{E}$, it is obvious that $\mathbf{E}$ is also parallel to the axis. Since the space charge is zero except in the electrode falls, $\nabla\cdot\mathbf{E}=0$, which yields the fact that $\mathbf{E}$ is independent of z. By application of the continuity equation for electric charge $\nabla\cdot\mathbf{j}=0$, Ohm's law, and $\nabla\times\mathbf{E}=0$ for steady state, one arrives at the conclusion that E is also independent of r.

Now, the thermal conduction potential is defined:

$$S=\int_{T_2}^{T}\lambda dT. \qquad (3)$$

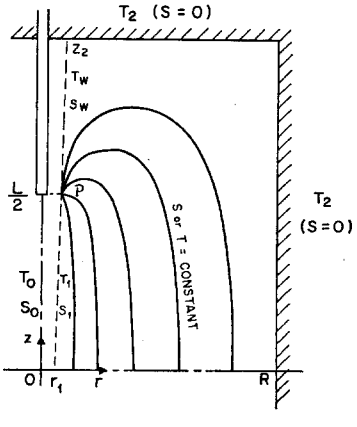

FIG. 4. Idealized model for gas temperature distribution in an arc chamber.

The energy equation may then be rewritten as

$$(1/r)(\partial/\partial r)[r(\partial S/\partial r)]+(\partial^2 S/\partial z^2)+\sigma E^2=0. \quad (4)$$

It is desired to linearize the $\sigma(S)$ function shown in Fig. 2 into the form

$$\sigma^*=B(S-S_1), \quad (5)$$

where σ^* is the linearized σ function, B is the slope of the straight line proposed to linearize the σ function, and S_1 is the reference value for S. Maecker[10] has proposed two methods for the determination of B and S_1: the integrated mean method and the minimum principle method. The former method gives

$$B=\sigma_0/(2S_0 f) \quad \text{and} \quad S_1=S_0(1-2f), \quad (6)$$

where

$$f=\int_0^{S_0}\sigma dS/(\sigma_0 S_0).$$

The latter method yields

$$B=(2f/9f_1^2)\sigma_0/S_0 \quad \text{and} \quad S_1=S_0(1-3f_1) \quad (7)$$

in which

$$f_1=\int_0^{S_0}\int_0^{S}\sigma dS dS \Big/ \left(S_0\int_0^{S_0}\sigma dS\right).$$

The integrated mean method which gave good agreement between the theoretical prediction and experimental results for a mercury arc[11] is employed in the present study.

With the linearized function σ^* available, the next step is to integrate the energy equation. In reference to Fig. 2 it is found that the solution may be easily obtained if the gas is divided into two regions: inner and outer regions. In the inner region where $S>S_1$, the conductivity σ^* is a finite value, while in the outer region where $S\leq S_1$, σ^* is identically zero. Since the wall is maintained isothermal and the needle electrodes are water cooled, our physical reasoning suggests that the actual temperature distribution may fall into the pattern shown in Fig. 3. The isothermal line through the arc axis is at temperature T_0. The corresponding thermal conduction potential is S_0. If the applied electric power is not too large there exists a region surrounding the arc axis in which all isothermal lines are parallel to the arc axis except at the arc column ends. The gas inside this region enclosed by an isothermal surface with temperature T_1 and the thermal conduction potential S_1 has the σ^*–S relationship as shown by the straight-line portion $S_1\sigma_0^*$ in Fig. 2, that is, the electric conductivity is directly proportional to $(S-S_1)$. This region is referred to as the inner region. The gas in the space outside the isothermal surface T_1 has zero electric conductivity for all values of S in $S_1\geq S\geq 0$ as shown by the $S_1 0$ line in Fig. 2 and is referred to as the outer region. For convenience in analysis, the temperature distribution pattern in Fig 3 is idealized as shown in Fig. 4. Now the isothermal surface T_1 is not a cone shape but a cylindrical surface with radius r_1. Point P in Fig. 4 is a point discontinuity from which all isothermal lines or surfaces are originating rather than from the electrode surface as shown in Fig. 3.

With this idealization in the temperature distribution pattern of the gas, the energy equation (2) may be rewritten as

$$(1/r)(d/dr)[r(dS_{\text{in}}/dr)]+\sigma^* E^2=0 \quad (8)$$

for the inner region $r_1\geq r\geq 0$ and $z\leq L/2$, and

$$\frac{1}{r}\frac{\partial}{\partial r}\left(r\frac{\partial S_{\text{out}}}{\partial r}\right)+\frac{\partial^2 S_{\text{out}}}{\partial z^2}=0 \quad (9)$$

for the outer region $r>r_1$. The appropriate boundary and matching conditions are

$$dS_{\text{in}}(0)/dr=0, \qquad S_{\text{in}}(r_1)=S_1 \quad (10a)$$

$$\partial S_{\text{out}}(r_1, z)/\partial r=dS_{\text{in}}(r_1)/dr \quad (10b)$$

$$S_{\text{out}}(r_1, z=S_1 \quad \text{for} \quad z\leq L/2$$
$$=SI \quad \text{for} \quad z>L/2 \quad (10c)$$

$$S_{\text{out}}(R, z)=S_{\text{out}}(r, z_2)=0 \quad (10d)$$

$$\partial S_{\text{out}}(r, 0)/\partial z=0 \quad (10e)$$

For a chamber of very large size, $R\to\infty$ and $z_2\to\infty$.

Equation (8) is integrated twice following the substitution of Eq. (5) for σ^*. It yields

$$S_{\text{in}}=S_1+(S_0-S_1)J_0[E(B)^{1/2}r], \quad (11)$$

where J_0 is the Bessel function of zeroth order. S_{in} of Eq. (11) satisfies

$$S_{\text{in}}(0)=S_0 \quad \text{and} \quad dS_{\text{in}}(0, z)/dr=0. \quad (12)$$

Equation (9) is solved by the method of separation of variables. The solution which satisfies the boundary and matching conditions (10b)–(10e) is

$$S_{\text{out}}=\sum_{m=0}^{\infty}\frac{2}{Z_2}\frac{K_0(\gamma_m r)-I_0(\gamma_m r)K_0(\gamma_m r)/I_0(\gamma_m r)}{K_0(\gamma_m r_1)-I_0(\gamma_m r_1)K_0(\gamma_m R)/I_0(\gamma_m R)}\left[\int_0^{z_2}F(Z')\cos\gamma_m Z' dZ'\right]\cos\gamma_m z, \quad (13)$$

where $\gamma_m=(m+1/2)\pi/z_2$, I_0, and K_0 are the modified Bessel functions of the zeroth order of the first and second kind, respectively, and the function $F(z)$ is defined as

$$F(z)=S_1 \quad \text{for} \quad z<L/2$$
$$=S_w \quad \text{for} \quad z>L/2. \quad (14)$$

If the chamber is very large in size, i.e., $R\rightarrow\infty$ and $z_2\rightarrow\infty$, Eq. (13) may be reduced to

$$S_{\text{out}}=\frac{2}{\pi}\int_0^\infty \frac{K_0(\omega r)\ \cos\omega z}{K_0(\omega r_1)}\left[\int_0^\infty F(Z')\ \cos\omega Z' dZ'\right]d\omega. \tag{15}$$

The special case where $T_w=T_2$ or $S_w=0$ is treated in the following to demonstrate the method for quantitative evaluation of the physical parameters such as the radius of the inner domain r_1, the electric field strength E, the current I, and the electric power delivered per unit length of the arc defined as

$$P=\int_0^R \sigma^* E^2 2\pi r dr. \tag{16}$$

For $T_w=T_2$ and $S_w=0$, Eqs. (13) and (15) may be reduced to

$$S_{\text{out}}=S_1\sum_{m=0}^{\infty}\frac{2}{\bar{z}_2}\frac{K_0(\Gamma_m\bar{r})-I_0(\Gamma_m\bar{r})K_0(\Gamma_m\bar{R})/I_0(\Gamma_m\bar{R})}{K_0(\Gamma_m\bar{r}_1)-I_0(\Gamma_m\bar{r}_1)K_0(\Gamma_m\bar{R})/I_0(\Gamma_m\bar{R})}\frac{\sin\Gamma_m\ \cos\Gamma_m\bar{z}}{\Gamma_m} \tag{17}$$

for a finite chamber and

$$S_{\text{out}}=\frac{2S_1}{\pi}\int_0^\infty \frac{K_0(\Omega\bar{r})}{K_0(\Omega\bar{r}_1)}\frac{\sin\Omega\ \cos\Omega\bar{z}}{\Omega}d\Omega \tag{18}$$

for a very large chamber, respectively. The dimensionless quantities are defined as $\bar{r}=2r/L$, $\bar{R}=2R/L$, $\bar{r}_1=2r_1/L$, $\bar{z}=2z/L$, $\Omega=\omega L/2$, and $\Gamma_m=\gamma_m L/2$.

Using Eqs. (11), (17), and (18), the boundary condition (10b) yields the expression for $\bar{r}_1$ or r_1:

$$\frac{12.231(S_0-S_1)}{\bar{r}_1}=\frac{2S_1}{\bar{z}_2}\sum_{m=0}^{\infty}\frac{\Gamma_m K_1(\Gamma_m\bar{r}_1)+\Gamma_m I_1(\Gamma_m\bar{r}_1)K_0(\Gamma_m\bar{R})/I_0(\Gamma_m\bar{R})}{K_0(\Gamma_m\bar{r}_1)-I_0(\Gamma_m\bar{r}_1)K_0(\Gamma_m\bar{R})/I_0(\Gamma_m\bar{R})}\frac{\sin\Gamma_m\ \cos\Gamma_m\bar{z}}{\Gamma_m} \tag{19}$$

for a finite chamber and

$$\frac{12.231(S_0-S_1)}{\bar{r}_1}=\frac{2S_1}{\pi}\left[\frac{d}{d\bar{r}}\int_0^\infty \frac{K_0(\Omega\bar{r})\ \sin\Omega\ \cos\Omega\bar{z}}{\Omega K_0(\Omega\bar{r}_1)}d\Omega\right]_{\bar{r}=\bar{r}_1} \tag{20}$$

for a very large chamber. Since the isothermal line at the region interface is parallel to the arc axis, its temperature gradient is independent of $\bar{z}$. As a result, $\bar{r}_1$ obtained from Eq. (19) or (20) is single valued.

The substitution of Eq. (11) into the second expression of the boundary condition (10a) leads to the relationship $J_0[E(B)^{1/2}r_1]=0$ or $E(B)^{1/2}r_1=2.405$. Hence, the electric field strength may be expressed as

$$E=2.405/(B)^{1/2}r_1. \tag{21}$$

The power delivered per unit length P can be determined either by Eq. (16) or by heat conduction from the arc column. The latter gives

$$P=-2\pi r_1(dS_{\text{in}}/dr)_{r=r_1}=7.84(S_0-S_1). \tag{22}$$

The current defined as P/E is obtained as

$$I=3.19r_1(B)^{1/2}(S_0-S_1). \tag{23}$$

RESULTS AND DISCUSSION

The thermal conductivity for a monatomic gas may be expressed as $\lambda=(3k/2\sqrt{2}Q_{aa})(8kT/\pi m_a)^{1/2}$, where m_a is the atomic mass, k is the Boltzmann constant, and Q_{aa} is the effective cross section between atoms. According to the definition, the thermal conduction potential is

$$S=2(kT)^{3/2}/Q_{aa}. \tag{24}$$

For weakly ionized gases, the electric conductivity is

$$\sigma=[e^2(2\pi kT)^{3/4}m_e^{1/4}/h^{3/2}Q_{ae}(3p)^{1/2}]\exp(-E_i/2kT),$$

where m_e is the electron mass, h is the Planck's constant, Q_{ae} is the effective cross section between atom and electron, E_i is the ionization energy, and p is the pressure. The electric conductivity may be expressed in term of S as

$$\sigma=[e^2(2m_e m_a)^{1/4}\pi/Q_{ae}h^{3/2}](Q_{aa}S/3p)^{1/2}\times\exp[-E_i/(2\pi m_a Q_{aa}^2)^{1/3}S^{2/3}].$$

For hydrogen, it is known that[19] $Q_{aa}=4\pi(10^{-16})$ (cm^2), $Q_{ae}=1.30(10^{-14})$ (cm^2) and $E_i=2.18(10^{-11})$ (erg).

For strongly ionized gases, the thermal and electric conductivities[20] are $\lambda=6.28(10^{50})k(kT)^{5/2}/\ln\Lambda$ (erg/cm·sec·°K) and $\sigma=0.865(10^{32})T^{3/2}/\ln\Lambda$ (1/sec) respectively, where $\ln\Lambda$ is the Coulomb logarithm, $\Lambda=kT/e^2n_e^{1/3}$ according to Ref. 19, and n_e is the electron density.

Numerical computations were carried out for a monatomic hydrogen arc contained in a very large chamber.

[19] H. Maecker, Th. Peters, and H. Schenk, Z. Physik **140**, 119 (1955).

[20] L. Spitzer, *Physics of Fully Ionized Gases* (Interscience Publishers, Inc., New York, 1956), p. 136.

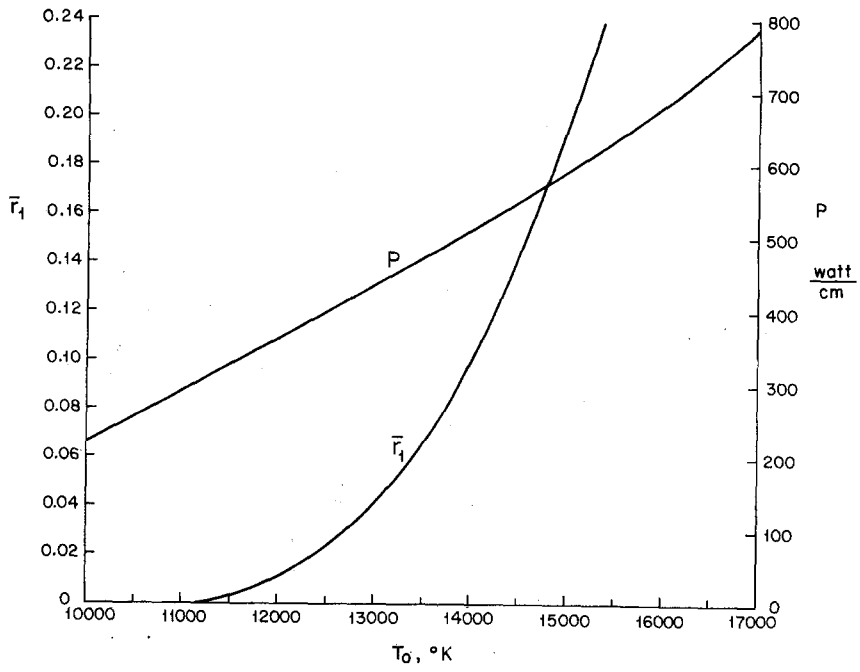

FIG. 5. The electric power and dimensionless radius of inner region as functions of arc-axis temperature for hydrogen arc under 1-atm pressure.

The hydrogen gas is maintained at 1 atm pressure. S_0 and σ_0 calculated for each specified T_0. S_1 was then determined using Eq. (6). Therefore, from Eq. (20) it can be seen that $\bar{r}_1$ depends only on T_0. The $\bar{r}_1-T_0$ relationship is graphically illustrated in Fig. 5. In order that the analysis be valid, the assumption of small $\bar{r}_1$ has to be satisfied. For the value of $\bar{r}_1=0.2$, Fig. 5 shows that T_0 is about 15 000°F. At this temperature the hydrogen gas is still weakly ionized. The electric power P calculated from Eq. (22) is superimposed in Fig. 5. It indicates a direct proportionality between P and T_0.

The distribution of the thermal conduction potential was calculated for $T_0=13\,000$°K and the arc length of 6 cm using Eqs. (11) and (18). Through the use of Eq. (24), the distribution was reduced to the gas temperature pattern as shown in Fig. 6. As a reference, Maecker's analytical result[10] for a constricted hydrogen arc with the arc-axis temperature of 13 000°F confined in an 1 cm radius tube is superimposed in the figure.

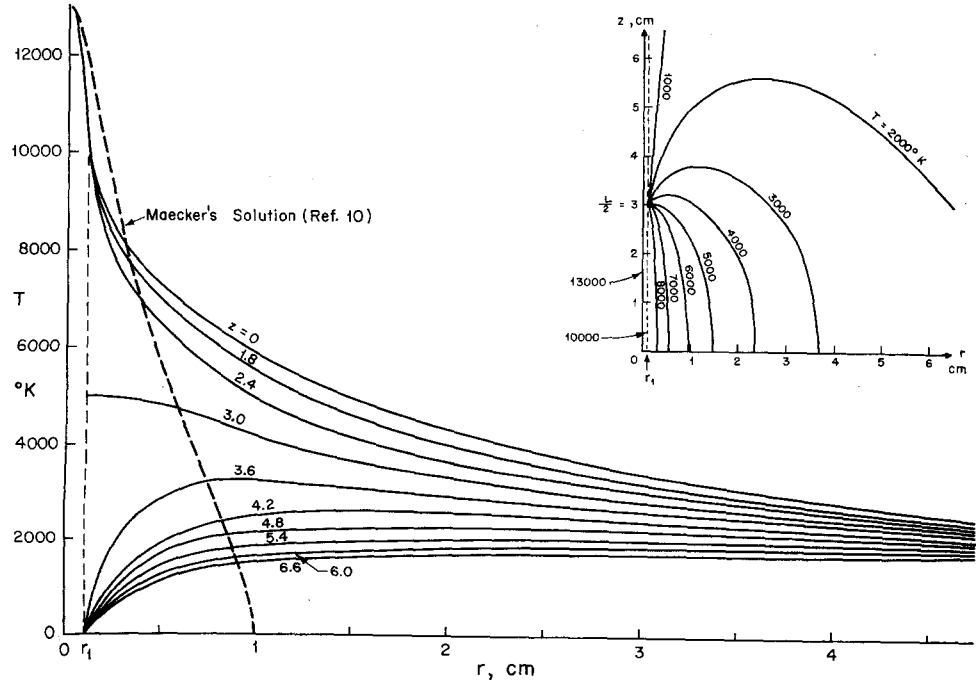

FIG. 6. Hydrogen temperature distribution in a very large chamber with a 6-cm long hydrogen arc.

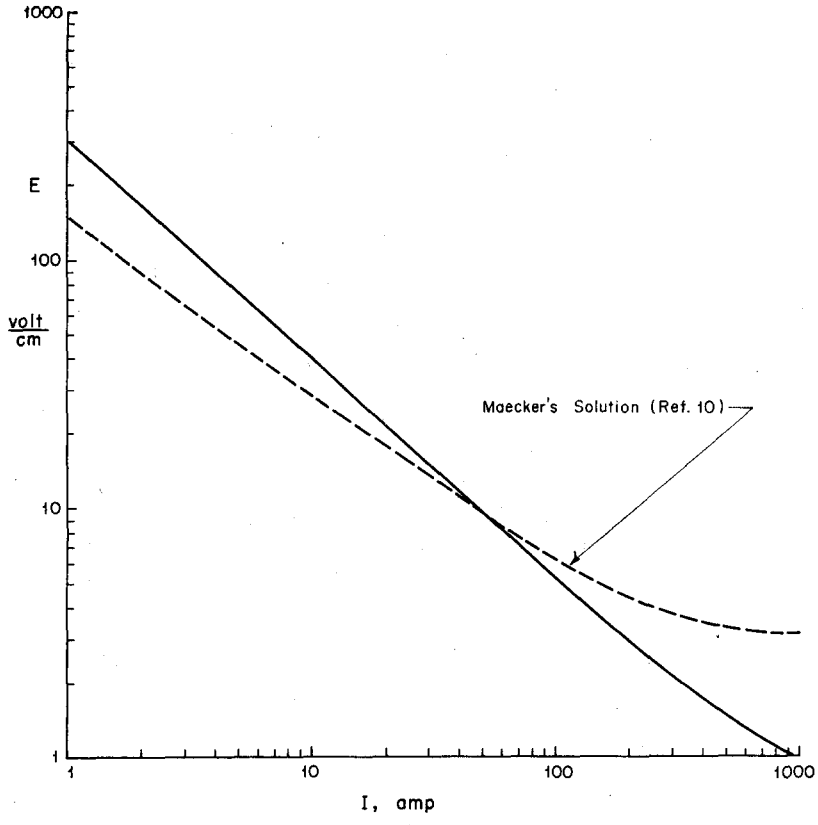

FIG. 7. Electric field strength vs current characteristics of a 6-cm long hydrogen arc in a very large chamber under one atmospheric pressure.

It is observed that the gas temperature gradients at small distances from the arc axis are larger in the present model than in Maecker's solution, whereas the temperature gradients become less steep away from the arc. It is worth while discussing the striking difference in the temperature gradients which can be reduced, eliminated, or even amplified depending on the geometry of an arc or a chamber. One may recall that T_1 is defined as the gas temperature at $r=r_1$, where the value of r_1 is related to the geometry of an arc or a

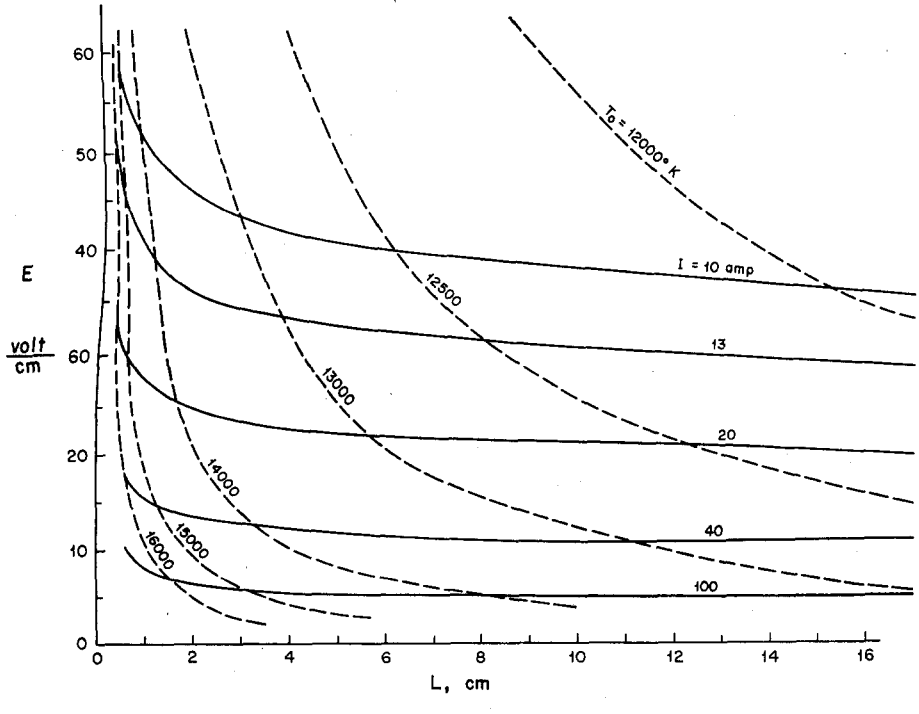

FIG. 8. The relationship among the electric field strength, current, arc-axis temperature, and arc length for a hydrogen arc in a very large chamber under 1-atm pressure.

chamber. For the Maecker's model, r_1 is related to the radius of arc chamber by

$$r_1 = R \exp[-S_1/1.2484(S_0 - S_1)], \quad (25)$$

while in the present model, r_1 is related to the arc length by

$$r_1 = \mathfrak{r}_1 L/2. \quad (26)$$

Therefore, for a specified arc-axis temperature T_0 one can change R and/or L such that the gas temperatures determined by the two models may become the same at the same value of r_1. In other words, if an arc with the length of 12 cm or an arc chamber with one-half of its original radius were used in Fig. 6, then the gas temperature gradients at small distances from the arc axis would be very close for the two models.

Figure 7 shows the electric field strength–current characteristics of the 6 cm long arc obtained from Eqs. (21) through (24). The Maecker's result is superimposed in the figure for reference. In the present model, one can find $E = 4.81/(B^{1/2}\bar{r}_1 L)$ and $I = 6.38 r_1 L(S_0 - S_1)B^{1/2}$ from Eqs. (21) and (23), respectively. This indicates that E is inversely proportional to L, while I is directly proportional to L. Therefore, an increase in an arc length will cause a decrease in the gradients of the E–I curve in Fig. 7. Similarly, in the Maecker's model, one finds in Ref. (10) that E is inversely proportional to R; I is directly proportional to R. Hence, an increase in the radius of an arc chamber will result in a decrease in the gradients of the E–I curve.

It is most interesting to examine the effects of the arc length on the arc-axis temperature, electric field strength, and current. The expression for the arc length may be obtained by the substitution of $E = P/I$ into Eq. (21) as

$$L = 4.81 I/[(B)^{1/2}\bar{r}_1 P]. \quad (27)$$

Since B, $\bar{r}_1$, and P are functions only of T_0, the current required to produce an arc with length L and axis temperature T_0 may be calculated using Eq. (25). The results are illustrated in Fig. 8. It is seen in the figure that a short arc requires higher electric field strength E. For the same current applied to a long arc the electric field strength will not change much with a change in the arc length. This is observed in experiments[14] if the following two assumptions are imposed on the interpretation of the results: (1) The electrode falls do not change appreciably with the arc length and (2) the arc length is sufficiently long that the electrode falls do not interfere with each other. Figure 8 also shows that for the same current, the arc-axis temperature decreases as the arc length is increased.

CONCLUDING REMARKS

An analysis was made for the gas temperature distribution in a long arc stabilized by vortex flow in a cylindrical chamber. Through the linearization of the electric conductivity–thermal conduction potential relationship together with the use of thermal conduction potential, analytical solutions were obtained for two regions. In the inner region corresponding to the arc core the gas temperature is independent of the distance along the core axis, while in the outer region the effect of the Joule heating is negligible. The solution thus obtained is valid for the case where the ratio of the arc-core radius to the arc length is small or equivalent for the case of relatively low arc-axis temperature.

A method was developed to determine the characteristics of the arc, notably the relationship among the electric field strength, arc length, current, and arc-axis temperature. Numerical computations were carried out for a monatomic hydrogen arc contained in a very large chamber. The results indicate that a short arc requires higher electric field strength, higher current, and higher arc-axis temperature than a long one. For the same current applied to a long arc, the electric field strength will not change much with a change in the arc length. The method developed in the study may also be applied to determine the characteristics of a rotationally stabilized long arc contained in a cylindrical chamber of finite size.

ACKNOWLEDGMENTS

The first author wishes to express his gratitude to the Institute of Science and Technology of the University of Michigan for a postdoctoral fellowship. Thanks are also due to Professor J. A. Clark of the University for valuable suggestions.